Influence of Organoclay and Preparation Technique on the Morphology of Polyamide6/Polystyrene/Organoclay Nanocomposites

Jintao Yang, Li Sun, Saifei Xiang, Jianlong He, Lianchao Gu, Mingqiang Zhong

College of Chemical Engineering and Material, Zhejiang University of Technology, Hangzhou 310014, People's Republic of China

Received 22 August 2006; accepted 7 November 2007
DOI 10.1002/app.28178
Published online 9 July 2008 in Wiley InterScience (www.interscience.wiley.com).

ABSTRACT: To have an improved insight about the compatibilization effect of organoclay on immiscible polymers, two different organoclays and preparation techniques were chosen to prepare polyamide6 (PA6)/polystyrene (PS)/organoclay ternary nanocomposites. The morphology analysis based on the results of X-ray diffraction, transmission electron microscopy, and scanning electron microscopy demonstrated that the type of organoclay and preparation technique had a significant influence on the dispersion and distribution of organoclay in the polymer. It was concluded that blending PS/organoclay nanocomposite synthesized previously via *in situ* bulk polymerization, with PA6 can realize the full exfoliation of organoclay in the final ternary nanocomposite, while an intercalated structure was achieved by directly blending the three components. The distribution of organoclay could be controlled by tuning the surface property of clay, and hence the interfacial interaction between clay and the polymer matrix. © 2008 Wiley Periodicals, Inc. J Appl Polym Sci 110: 276–282, 2008

Key words: morphology; ternary nanocomposite; preparation technique

INTRODUCTION

Polymer blends and alloys have become one of the most popular approaches to produce new high performance materials because they show remarkable enhancement of mechanical properties, and exhibit some unique physical or chemical properties when compared with the corresponding individual polymers.[1–4] In the processing of polymer blends and alloys, especially in the processing of immiscible polymer blends, the compatibilizer, which can manipulate the interfacial properties of the polymer pairs, improve the interfacial interaction and remarkably reduce the dispersion domains size,[5–7] is the key concern for both industrial production and academic research.

Polymer/inorganic nanocomposites, especially polymer/clay nanocomposites have attracted a lot of attention in the materials science field.[8–10] Because of the high aspect ratio and strong interaction with polymer matrix, clay often offers the polymer matrix a higher modulus, higher tensile strength, and lower permeability. Recently, besides its extensive application in one-component polymer matrix, organoclay has also been studied as a potential additive in the two-component matrix since it has a good compatibilization effect on the immiscible polymer pairs.[11] Ray and Bousmina[12] reported that the organoclay could act as a compatibilizer in polymethyl methacrylate (PMMA)/polycarbonate (PC) blend. The dispersed PC domain size was reduced and the interaction between PMMA and PC was dramatically enhanced. Wang et al.[13] also observed that the domain size of polypropylene (PP) dispersed in polystyrene (PS) was substantially reduced by the addition of organoclay. They attributed the compatibilization effect to the chains of the immiscible polymer pair cointercalated into the gallery of clay, which make clay act as a block copolymer. This mechanism, however, can only be applied to explain the situation in which the clay is dispersed in the polymer blends as an intercalated structure. Moreover, Ray and Bousmina[14] viewed that the strong adsorption of both the parent polymers on the clay increased the compatibility and interaction of the immiscible polymer pairs.

According to previous studies, most researches focused on the compatibilization effect of organoclay on different polymer pairs but few studies have been done to control the morphology of ternary nanocomposites.[15–18] The present study is aimed at investigating the influence of different organoclays and preparation techniques on the morphology of polyamide6 (PA6)/PS/organoclay ternary nanocomposite

Correspondence to: M. Zhong (zhongmq@zjut.edu.cn).
Contract grant sponsor: the Doctor Preliminary Foundation of Zhejiang University of Technology.

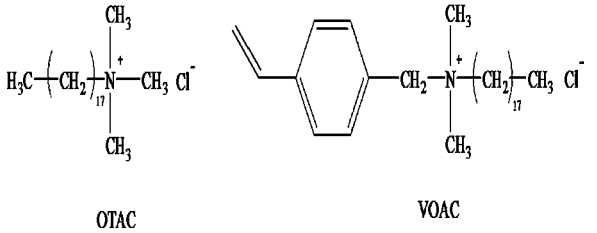

Figure 1 The chemical structure of the surfactant OTAC and VOAC.

and to provide a way to control the distribution of organoclay in the polymer pairs. To realize this objective, two kinds of organoclay (C_{18}–MMT and VC_{18}–MMT) synthesized by exchanging inorganic cations with trimethyloctadecyl ammonium chloride (OTAC) and vinylbenzyldimethyloctadecyl ammonium chloride (VOAC) were chosen. PS/organoclay nanocomposites were initially synthesized via *in situ* bulk polymerization and afterwards blended with PA6 to obtain the ternary nanocomposites. For comparison, the ternary nanocomposite was also prepared by directly blending the three components. The microstructure of nanocomposites was characterized by a combination of X-ray diffraction (XRD), transmission electron microscopy (TEM), and scanning electron microscopy (SEM).

EXPERIMENTAL

Materials

Clay with naturally hydrophilic property was supplied by Huate Clay Company, Zhejiang China. The cation exchange capacity of the clay used in this study is 105 mequiv/100 g. OTAC was purchased from Jingwei Chemical Company and was used as received. VOAC was synthesized in our lab following the method reported by Fu.[19,20] The chemical structures of ammoniums are shown in Figure 1. Organoclay was obtained by exchange reaction between the inorganic cation (Na^+) in the gallery of original clay and ammonium. The procedure is described in detail elsewhere.[21,22] Styrene was purified by distillation under reduced pressure and the initiator 2,2–azobi(isobutyronitrile) (AIBN) was purified by re-crystallization from alcohol.

The PA6 with trade name 1013B used in this study was purchased from Mitsubishi Industries.

PS and PS/Organoclay nanocomposites preparation

In situ bulk polymerization was employed to synthesis the PS/organoclay nanocomposites in our study. Ultrasonication was used to facilitate predispersion of organoclay in styrene.

A specific amount of organoclay (C_{18}-MMT or VC_{18}-MMT) was added into styrene, before polymerization. The suspension was stirred for 4 h and sonicated for 15 min in an ice/water bath. Then, the initiator, AIBN (0.2 wt % of monomer) was added into the suspension. The polymerization was carried out isothermally at 70°C for 15 h and the product was postcured at 100°C for 5 h to complete the reaction. The final solid product was milled into powder and washed with hot alcohol to remove the remaining styrene monomer. The nanocomposites were dried under reduced pressure at 70°C for 10 h and marked as PS/C_{18}-MMT and PS/VC_{18}–MMT.

Ternary nanocomposites preparation

The ternary nanocomposites were obtained by blending the PS/organoclay nanocomposites with PA6 or directly blending PS, organoclay and PA6. The mixing was performed in a twin rotor Thermohaake-mixture (thermo 90). The blending temperature, blending time and rotor speed were set at 220°C, 8 min, and 80 rpm, respectively. The marks and blending designation of compounds are shown in the Table I.

Measurements

The XRD patterns were recorded on a Leitz Wetzlab diffractometer with Cu radiation (36 kV, 30 mA). Data was obtained from $2\theta = 1$–10° at a scanning speed and step size of 2°/min and 0.02°, respectively. The interlayer spacing of organoclay was calculated using the Bragg equation.

TABLE I
The Formulations of Compounds Blended in Haake-Mixture

	Blending ingredient (wt %)				
Samples	PA6	PS	PS/C_{18}-MMT	PS/VC_{18}-MMT	C_{18}-MMT
N1	70	30	–	–	–
N2	70	–	30 (6.7)*	–	–
N3	70	–	–	30 (6.9)*	–
N4	70	28	–	–	2

* The numbers in the bracket represent the actual organoclay content (%) in the nanocomposites.

The morphology of PS/oganoclay nanocomposites and ternary nanocomposites was obtained on a JEM-1200EX TEM operating at an accelerating voltage of 80 kV. The samples were cut into ultra thin slices using a microtome equipped with a diamond knife at ambient temperature.

To study the surface properties of clay in PS/organoclay nanocomposites, the nanocomposites were extracted by hot tetrahydrofuran. The remaining weight of nanocomposites was used to calculate the ratio of PS grafted on clay layers through equation as follow:

$$\chi = \frac{W_e - W_t \times a}{W_t \times (1 - a)} \times 100\%$$

where χ is the ratio of PS grafted on the clay layers, W_e is the mass weight of nanocomposite after extraction, W_t is the total weight of nanocomposite, and a is the weight fraction of clay in nanocomposite. The average molecular weight and molecular weight distribution of extracted polymer were determined by Waters-150 gel permeation chromatography (GPC) at 30°C with a THF flow rate of 1.0 mL/min.

The stick samples of ternary nanocomposites were cryo–fractured in liquid nitrogen. The fracture surfaces were etched with toluene at ambient temperature for 24 h to remove the dispersed PS phase. The etched surfaces were sputter-coated with gold and examined with a Hitachi *S*–4700 SEM. The resulting micrographs were analyzed using image analysis software to determine the dispersed PS domains size distribution. A minimum number of 150 PS caves in each micrograph were counted.

The melt viscosity of the ternary nanocomposites (shear rate from 50 to 1000 s^{-1}) was characterized using a Rosand RH7 capillary rheometer at a temperature of 220°C.

RESULTS AND DISCUSSION

Microstructure of PS/organoclay nanocomposites

Two kinds of PS/organoclay nanocomposites containing around 7.0 wt % of organoclay were synthesized via *in situ* bulk polymerization. Figure 2 shows the XRD patterns of the nanocomposites. In the XRD pattern of PS/C_{18}–MMT, a characteristic peak of clay is observed at $2\theta = 2.76^\circ$, corresponding to an interlayer spacing of 3.23 nm. In our previous study,[21] the interlayer spacing of pure C_{18}-MMT was determined as 2.0 nm. The increased interlayer spacing indicates the intercalation of PS chains into the galleries of clay and thus, an intercalated nanocomposite is formed. For PS/VC_{18}–MMT, no characteristic peak is found, implying the full exfoliation and random dispersion of clay in polymer matrix.

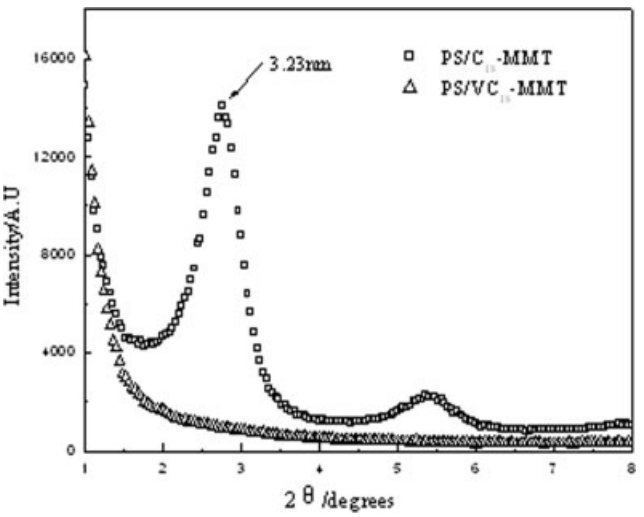

Figure 2 The XRD patterns of PS/C_{18}-MMT and PS/VC_{18}-MMT nanocomposites.

Although XRD offers a convenient method to determine the interlayer spacing of clay in the intercalated nanocomposites (within 1–4 nm), little can be said about the spatial distribution of clay, or any structural nonhomogeneities. Additionally, some kinds of clay initially do not exhibit well-defined basal reflections. Thus, it is difficult to get to a conclusion about the mechanism of nanocomposites formation and their structure, based solely on XRD patterns. On the other hand, TEM allows a qualitative understanding of the internal structure, spatial distribution and dispersion of nanoparticles through direct visualization.[22] Figure 3(a, b) shows the typical TEM micrographs of PS/C_{18}–MMT and PS/VC_{18}–MMT. Although the two kinds of organoclays are similarly predispersed in the styrene monomer via ultrasonication, their dispersions in the final nanocomposites are distinctly different. VC_{18}–MMT is fully exfoliated into individual layers and randomly dispersed in the PS matrix, as illustrated in Figure 3(b), while C_{18}–MMT is dispersed as tactoids with thickness of about 10–20 nm, shown in Figure 3(a). The dispersion state of C_{18}-MMT can be attributed to the aggregation of clay layers during the polymerization, especially in the early stage of polymerization in which the viscosity of system is relative lower. However, the vinylbenzyl attached on the surfaces of VC_{18}–MMT layers can react with styrene, which has been confirmed by earlier studies.[19,23] The energy produced by copolymerization can facilitate the exfoliation of clay layers.

The results of extraction and the average molecular weight of PS extracted are listed in Table II. From the table, few remnants of PS/C_{18}–MMT after extraction are observed since there is no chemical bond between PS molecules and the clay layers. On

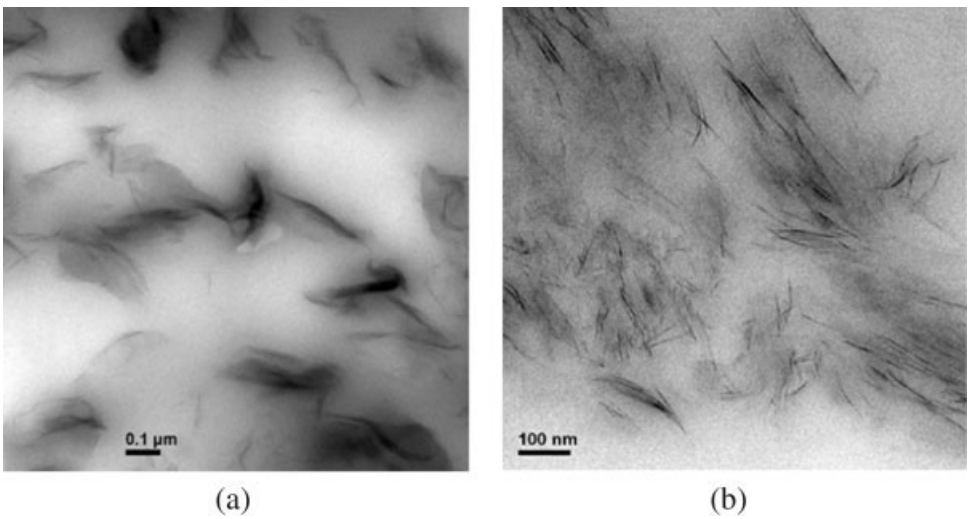

Figure 3 The typical TEM micrographs of PS/C_{18}-MMT (a) and PS/VC_{18}-MMT (b) nanocomposites.

the other hand, for PS/VC_{18}-MMT, there is a considerable amount of unextractable organic materials which can be regarded as the PS grafted on the VC_{18}–MMT layers by chemical bond. Moreover, the average molecular weight and molecular distribution of extracted PS from PS/C_{18}–MMT is almost similar to that of pure PS. On the contrary, the VC_{18}–MMT significantly decreases the molecular weight of PS. This maybe due to the fact that VOAC can copolymerize with styrene, making the chain transfer or chain termination more pronounced.

Morphology of ternary nanocomposites

Figure 4 shows the XRD patterns of ternary nanocomposites. It can be seen that the preparation technique has substantial influence on the dispersion of organoclay in the polymer matrix. The characteristic peak of clay is not observed in the patterns of N2 and N3, indicating an exfoliated structure. However, there is a broad peak at $2\theta = 2.7^\circ$, attributable to an interlayer spacing of 3.46 nm in the XRD pattern of N4, which suggests that the C_{18}-MMT exists in the nanocomposite as an intercalated structure. The different dispersion states of organoclay demonstrate that the technique of blending PS/organoclay nanocomposites and PA6 has the advantage of facilitating the exfoliation of clay.

TABLE II
The Molecular Weight and Molecular Weight Distribution of PS Extracted from PS/C_{18}-MMT and PS/VC_{18}-MMT

Samples	χ (%)	M_w	M_n	M_w/M_n
PS	–	13.82	4.63	2.98
PS/C_{18}-MMT	2.36	12.61	3.98	3.17
PS/VC_{18}-MMT	29.6	8.83	2.01	4.39

As mentioned above, to obtain the distribution of clay in the polymer pair, TEM analysis is carried out to observe the microstructure of nanocomposites. The micrographs of ternary nanocomposites are presented in Figure 5. In the micrographs, PA6, PS, and organoclay are easily distinguishable due to the contrast difference between them. The white ellipsoids are attributed to the dispersed PS domains, the gray continuous phase corresponds to the PA6 and the black lines are the layers of organoclay. The micrographs reveal that the distributions of C_{18}–MMT in N2 and N4 are almost similar. Most of the C_{18}–MMT layers are located in the PA6 component and at the interface between PA6 and PS while few exist in the PS component. The sole explanation is that the C_{18}-MMT layers prefer to exist in the PA6 component rather than the PS component. Even though similar microstructure is exhibited in N2 and N4, different

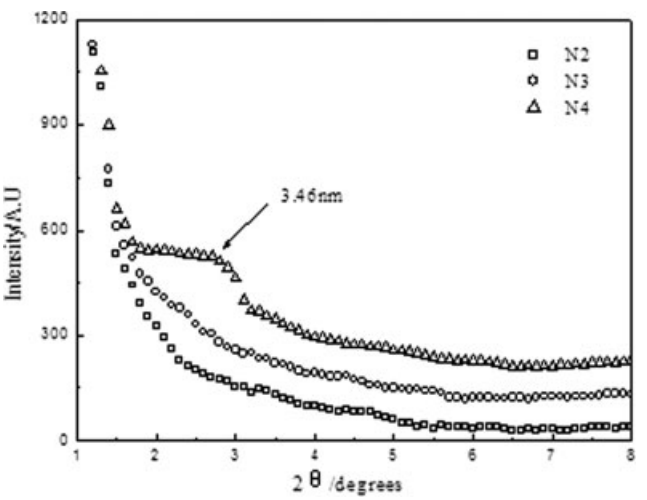

Figure 4 The XRD patterns of PA6/PS/Organoclay ternary nanocomposites.

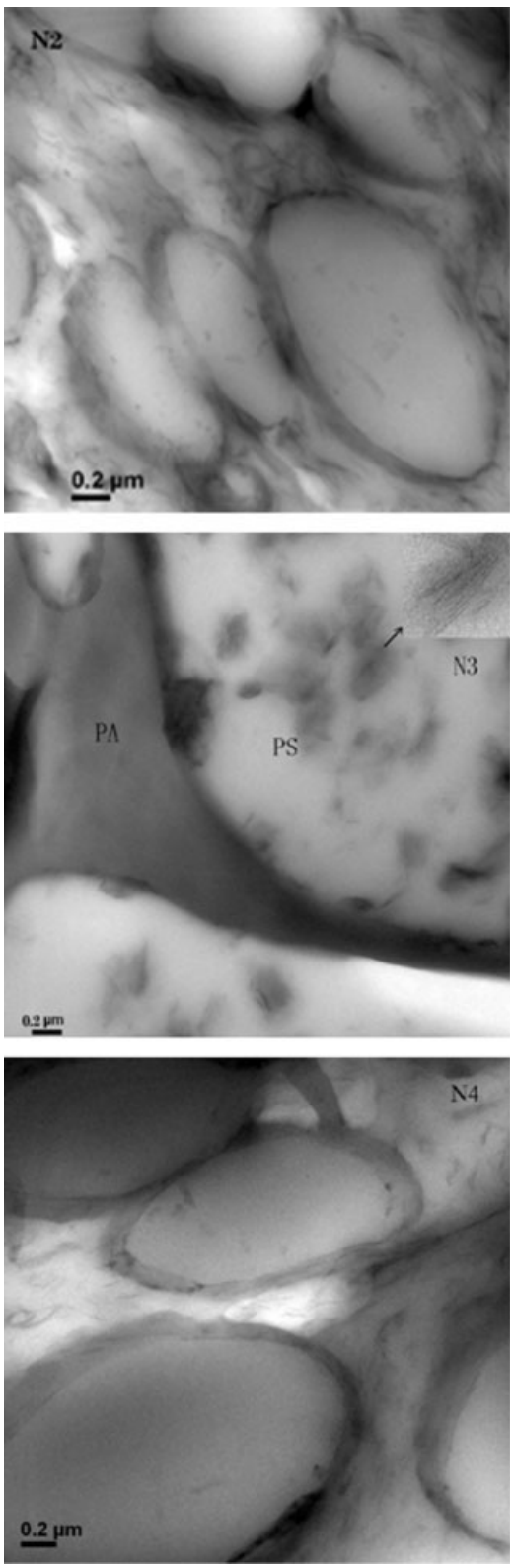

Figure 5 The typical TEM micrographs of ternary nanocomposites.

dispersed PS domain sizes in the two nanocomposites can be observed. The size of PS domains in N2 is much smaller than that in N4. Moreover, compared with N2 and N4, the VC_{18}–MMT layers exhibit an opposite distribution in N3. Except a small quantity of layers located at the interface, most VC_{18}-MMT layers are present in PS component. The reason for this morphology may be explained as follows. During the polymerization, the vinylbenzyl attached on the surface of VC_{18}–MMT layers can react with styrene and thus the PS chains can directly grow from the layers, which make the layers more compatible and have strong chemical interaction with PS matrix. Thus, most VC_{18}-MMT layers remain in the PS phase after blending due to the strong interfacial interaction.

Figure 6 presents the SEM micrographs taken from the cryo-fractures of N1-N4. In the images, the black caves are extracted PS domains. It can be clearly seen that the size of dispersed PS domains is dramatically reduced by the organoclay, suggesting the compatibilization effect of organoclay. Meanwhile, the size of dispersed PS domains in nanocomposites is also affected by the preparation technique and the surface property of clay. To obtain a qualitative comparison, we use the image analysis program to determine the dispersed PS domain size distribution in the different ternary nanocomposites. Figure 7 presents the dispersed PS domain size distribution in N1–N4. The calculated mean sizes of dispersed PS domains in N1, N2, N3, and N4 are 47, 13, 30, and 16 μm, respectively.

Previously, some studies[12,13] attributed the reduction of dispersed domain size to the increase of blend viscosity and cointercalation of polymer pairs in the interlayer spacing of clay. The viscosity of blend N1–N4 at the temperature of 220°C, as a function of shear rates is shown in Figure 8. Clearly, the viscosity of PA6/PS blend is increased by the addition of organoclay. However, even though the N3 blend has the maximum viscosity, the size of dispersed PS in it is not the minimum. Allowing for the full exfoliation (illustrated in Figs. 4 and 5) of organoclays in N2 and N3, no factor described above can be applied to explain the compatibilization effect of organoclay in this study. So we consider that the compatibilization effect of organoclay in this study might be explained as follows. Even though the clay is organically modified, it may preserve a part of its polar nature. So the organoclay layers with both hydrophilic and hydrophobic properties can act as true compatibilizer in the blend of PA6 and PS, which can be approved by the phenomenon that plenty of C_{18}-MMT layers are located at the interface between the two components. On the contrary, the VOAC attached on the surface of VC_{18}-MMT can react with styrene monomer. So the clay layers are coated with PS chains and become fully hydrophobic. During the blending, the VC_{18}–MMT layers remain in the PS component due to their compatibility

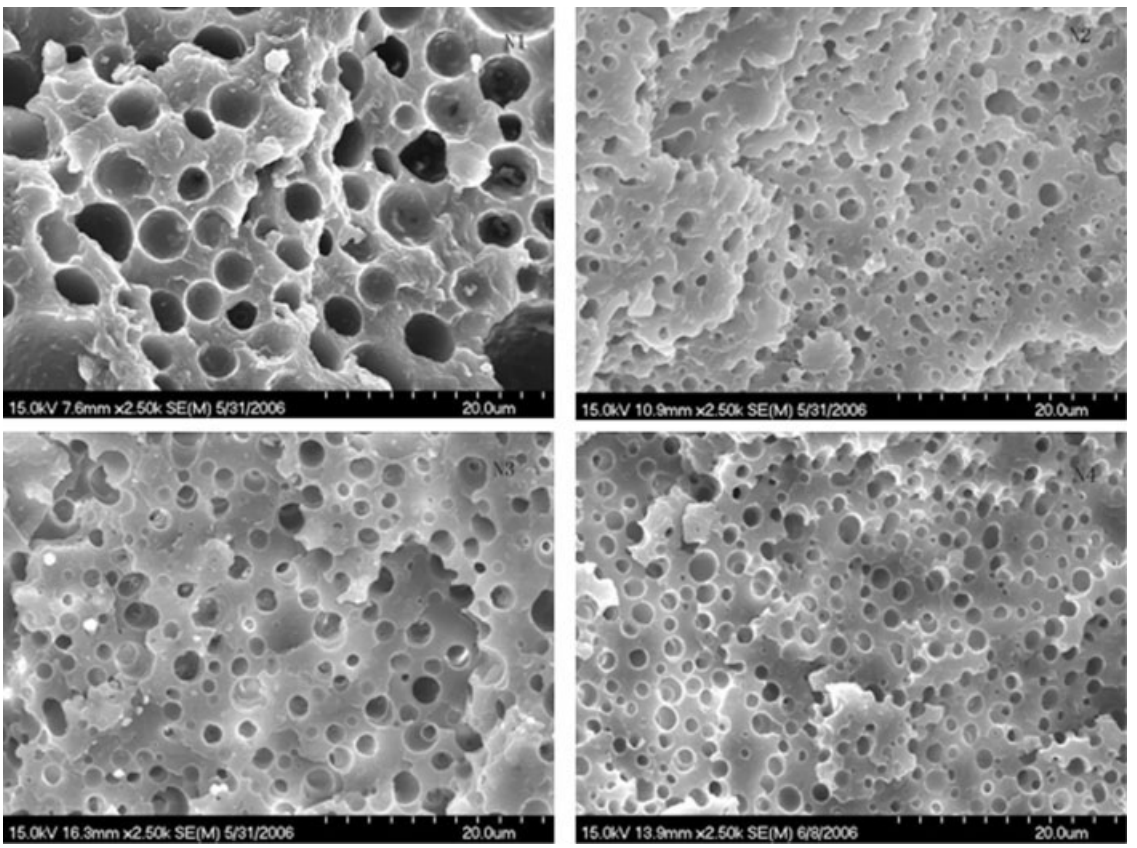

Figure 6 The typical SEM micrographs of fractures of ternary nanocomposites.

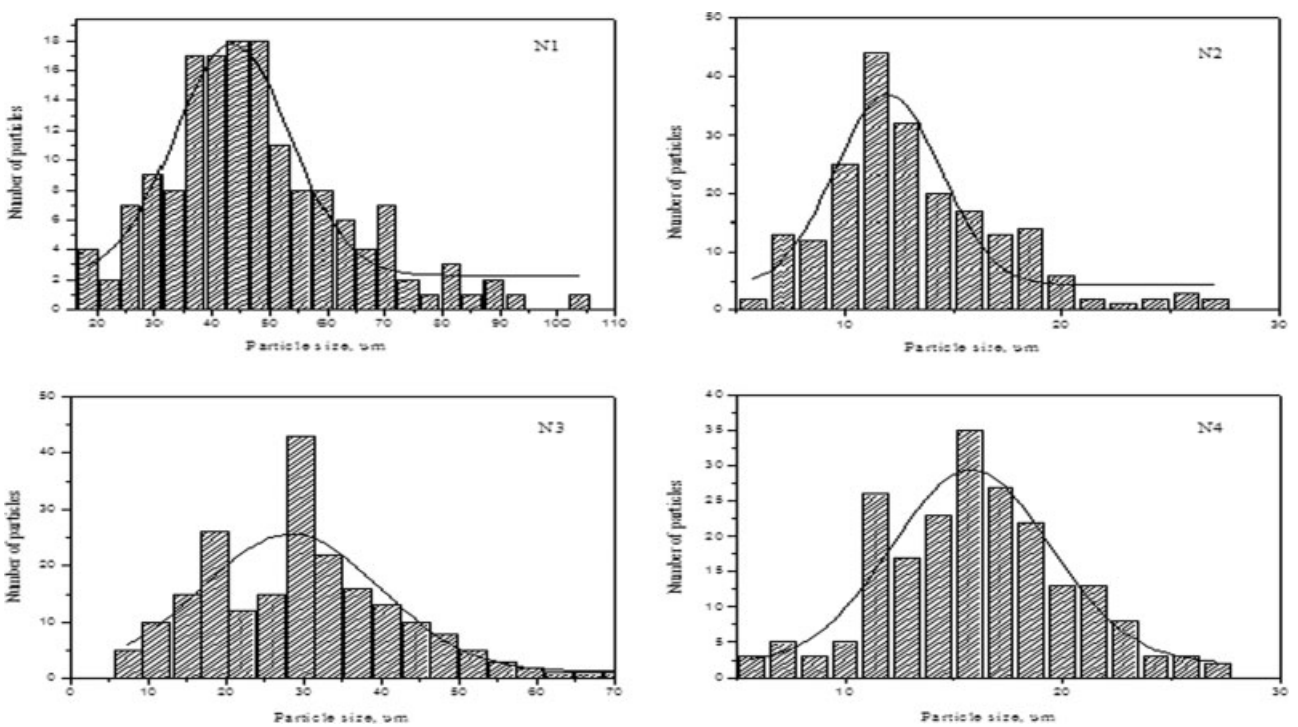

Figure 7 The dispersed PS domain size distribution in ternary nanocomposites.

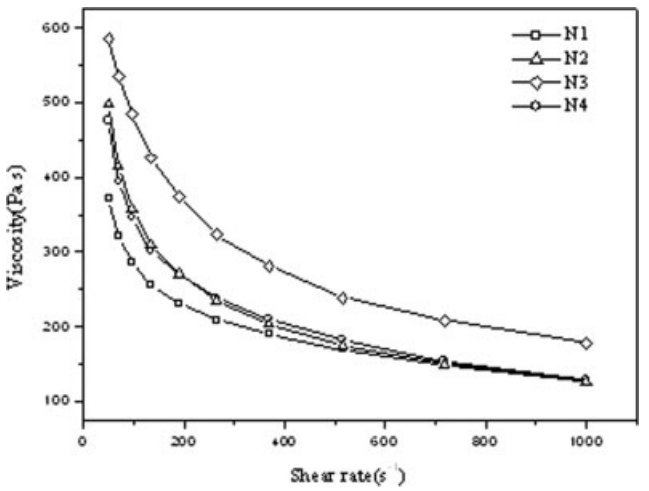

Figure 8 The melt viscosity of ternary nanocomposites at 220°C as a function of shear rate.

and strong interaction with PS. At the same time, the strong interaction between VC_{18}-MMT layers and PS offers the PS/VC_{18}–MMT nanocomposite with high melt viscosity. According to the results of melt flow index (MFI) determined at 200°C, the MFI of PS/VC_{18}-MMT nanocomposite is only 0.1 g/10 min, which is much lower than that of pure PS (7.0 g/10 min) and PS/C_{18}–MMT(2.5 g/10 min) nanocomposite. A lot of studies have shown that the viscosity ratio between the polymer pair had significant influence on the microstructure of polymer blend. So we consider that the exorbitant melt viscosity impedes the dispersion of PS in PA6, which in turn, causes the increased sizes of dispersed PS domains in N3 compared with N2 and N4. Although the optimal compatibilization effect is not achieved when we apply the VC_{18}–MMT copolymerized with styrene into the blends of PA6 and PS, it supplies us with the evidence that the distribution of organoclay in the polymer pairs can be controlled by tuning the surface property of clay.

CONCLUSIONS

This study demonstrated the influence of clay and preparation technique on the microstructure of PA6/PS/Organoclay ternary nanocomposites. It was shown that the distribution of organoclay in the polymer pairs was mainly determined by the surface property of clay layers. When the C_{18}–MMT was initially dispersed in the PS phase via *in situ* bulk polymerization and afterwards blended with PA6, the minimum mean size of dispersed PS domains was achieved. Although the VC_{18}–MMT grafted with PS chains did not show the desired compatibilization effect, it was shown that the microstructure and distribution of clay layer in polymer pairs could be controlled by tuning the surface properties of clay layers.

The authors thank Ms. Ying Xu in Zhejiang University for sample characterization and helpful discussion.

References

1. Liu, J.; Zhang, J. G. Polym Adv Technol 2003, 14, 337.
2. Hachiya, H.; Takayama, S.; Takeda, K. J Appl Polym Sci 1998, 70, 2521.
3. Hisamatsu, T.; Nakano, S.; Adachi, T.; Ishikawa, M.; Iwakura, K. Polymer 2000, 41, 4803.
4. Sawhney, G.; Gupta, S. K.; Misra, A. J Appl Polym Sci 1996, 62, 1395.
5. Xie, H. Q.; Liu, D.G.; Xie, D.; Guan, J. G. J Appl Polym Sci 2006, 95, 1887.
6. Seo, Y.; Kim, H. J.; Kim, Y. J.; Rhee, H. W. Polym Eng Sci 2002, 42, 951.
7. Zhang, X. M.; Tasaka, S.; Inagaki, N. Macromol Rapid Commun 1999, 20, 459.
8. Giannelis, E. P. Appl Organometal Chem 1998, 12, 675.
9. Giannelis, E. P. Adv Mater 1996, 8, 29.
10. Sinha, R. S.; Yamada, K.; Okamoto, M.; Ueda, K. Polymer 2003, 44, 857.
11. Gelfer, M. Y.; Song, H. H.; Liu, L. Z.; Hsiao, B. S.; Chu, B.; Rafailovich, M.; Si, M. Y.; Zaitsev, V. J Polym Sci Part B: Polym Phys 2003, 41, 44.
12. Ray, S. S.; Bousmina, M. Macromol Rapid Commun 2005, 26, 450.
13. Wang, Y.; Zhang, Q.; Fu, Q. Macromol Rapid Commun 2003, 24, 231.
14. Ray, S. S.; Bousmina, M. Macromol Rapid Commun 2005, 26, 1639.
15. Dasari, A.; Yu, Z. Z.; Mai, Y. W. Polymer 2005, 46, 5986.
16. Feng, M.; Gong, F. L.; Zhao, C. G.; Chen, G. M.; Zhang, S. M.; Yang, M. S. Polym Int 2004, 53, 1529.
17. Chen, G. X.; Kim, H. S.; Kim, E. S., Yoon, J. S. Polymer 2005, 46, 11829.
18. Ray, S. S.; Pouliot, S.; Bousmina, M.; Utracki, L. A. Polymer 2004, 45, 8403.
19. Fu, X.; Qutubuddin, S. Polymer 2001, 42, 807.
20. Qutubuddin, S.; Fu, X. A.; Tajuddin, Y. Polym Bull 2002, 48, 143.
21. Yang, J. T.; Fan, H.; Bu, Z. Y.; Li, B. G. Acta Materiae Compositae Sinica 2005, 2, 38.
22. Ray, S. S.; Bousmina, M. Progr Mater Sci 2005, 50, 962–1079.
23. Fu, X.; Qutubuddin, S. Mater Lett 2000, 41, 12.